AD-A039 829 DAVID W TAYLOR NAVAL SHIP RESEARCH AND DEVELOPMENT CE--ETC F/G 1/3
PERFORMANCE PREDICTION METHOD FOR A WING-IN-GROUND EFFECT VEHIC--ETC(U)
MAR 77 D G ROUSSEAU, R W GALLINGTON

UNCLASSIFIED DTNSRDC/ASED-379 NL

1 OF 1
AD A039 829

END

DATE FILMED
6-77

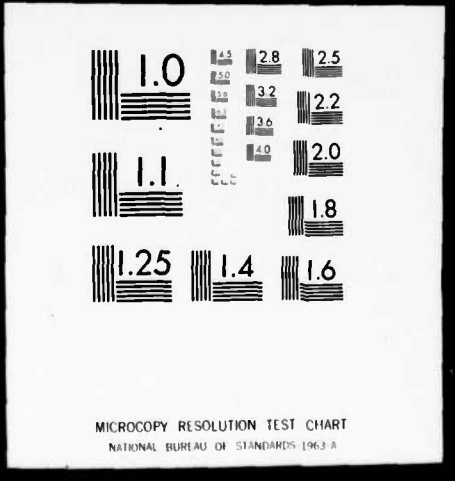

12

PERFORMANCE PREDICTION METHOD FOR A WING-IN-GROUND EFFECT VEHICLE WITH BLOWING UNDER THE WING

by

David G. Rousseau and Roger W. Gallington

AVIATION AND SURFACE EFFECTS DEPARTMENT

ASED 379

March 1977

DAVID W. TAYLOR NAVAL SHIP RESEARCH AND DEVELOPMENT CENTER

BETHESDA
MARYLAND
20084

(9) Final rept. Sep 76 - Mar 77.

UNCLASSIFIED

SECURITY CLASSIFICATION OF THIS PAGE (When Data Entered)

REPORT DOCUMENTATION PAGE

READ INSTRUCTIONS BEFORE COMPLETING FORM

(14) 1. REPORT NUMBER: DTNSRDC/ASED-379

2. GOVT ACCESSION NO.

3. RECIPIENT'S CATALOG NUMBER

(6) 4. TITLE (and Subtitle): PERFORMANCE PREDICTION METHOD FOR A WING-IN-GROUND EFFECT VEHICLE WITH BLOWING UNDER THE WING.

5. TYPE OF REPORT & PERIOD COVERED: Final (Sep 1976 - Mar 1977)

6. PERFORMING ORG. REPORT NUMBER

(10) 7. AUTHOR(s): David G./Rousseau and Roger W./Gallington

8. CONTRACT OR GRANT NUMBER(s): (16) SH15 (17) SFSH15002

9. PERFORMING ORGANIZATION NAME AND ADDRESS: Aviation and Surface Effects Department, David W. Taylor Naval Ship R&D Center, Bethesda, Maryland 20084

10. PROGRAM ELEMENT, PROJECT, TASK AREA & WORK UNIT NUMBERS: Program Element 63534N, Task Area SSH 15002, Work Unit 1612-008

11. CONTROLLING OFFICE NAME AND ADDRESS: ANVCE Project Office (NOP-96V), Rm 800 Commonwealth Bldg., 1300 Wilson Blvd, Arlington, VA 22209

(11) 12. REPORT DATE: March 1977

13. NUMBER OF PAGES: 29 (12) 36p.

14. MONITORING AGENCY NAME & ADDRESS (if different from Controlling Office)

15. SECURITY CLASS. (of this report): UNCLASSIFIED

15a. DECLASSIFICATION DOWNGRADING SCHEDULE

16. DISTRIBUTION STATEMENT (of this Report)

Approved for Public Release: Distribution Unlimited

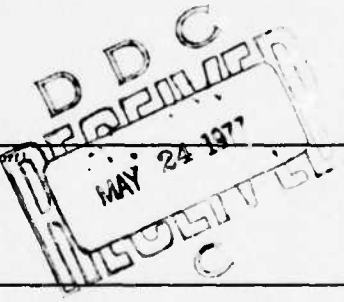

17. DISTRIBUTION STATEMENT (of the abstract entered in Block 20, if different from Report)

18. SUPPLEMENTARY NOTES

19. KEY WORDS (Continue on reverse side if necessary and identify by block number)

Wing-In-Ground Effect
Power Augmentation
Computer Performance Program

387695

20. ABSTRACT (Continue on reverse side if necessary and identify by block number)

Recent efforts in theoretical analysis and experimental observations have moved the concept of power-augmented flight in ground effect toward practicality. With the addition of lift and drag due to external airflow, end-plate leakage, water skin friction, wave drag effects, and wave clearance constraints, a flow model can be made capable of effective comments. The analysis shows that there are wave drag and wave clearance related limits to many aspects of the vehicle configuration. The most important of which are cruising height →

(Continued on reverse side)

DD FORM 1 JAN 73 1473 EDITION OF 1 NOV 65 IS OBSOLETE S/N 0102-014-6601

UNCLASSIFIED

SECURITY CLASSIFICATION OF THIS PAGE (When Data Entered)

and aspect ratio, in that they have a very large effect on transport efficiency. Unfortunately, the low flying high aspect ratio cases are ruled out due to wave impact problems. Testing of a point design vehicle, arrived at through the use of an analysis such as the one of this report, needs to be performed as final verification of the accuracy of the design procedure.

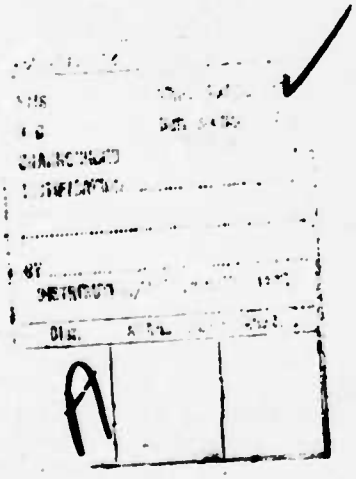

TABLE OF CONTENTS

LIST OF FIGURES

LIST OF TABLES

NOTATION

The final forms of the equations in the analysis used only dimensionless coefficients and ratios. However, during the derivation the U.S. Customary System of Units was used as an anchor for maintaining consistency of units. Equivalent values in the international System of Units (SI) are indicated parenthetically.

A,B	Wave drag curve fit coefficients
A_f	Channel entrance area, ft^2 (m^2)
A_j	Fan disk area, ft^2 (m^2)
A_s	Area of sidewall gap, ft^2 (m^2)
A_{te}	Area of trailing edge gap, ft^2 (m^2)
A_w	Submerged or emersed area of sidewall, ft^2 (m^2)
C_{DP}	Coefficient of vehicle form drag, $d_f/\frac{1}{2}\rho_a V_\infty^2 S$
C_f	Friction coefficient for water, $d_w/\frac{1}{2}\rho_w V_\infty^2 A_w$
C_{fa}	Friction coefficient for air, $d_a/\frac{1}{2}\rho_a V_\infty^2 S$
C_L	Lift coefficient, $L/\frac{1}{2}\rho_a V_\infty^2 S$
C_p	Pressure coefficient under the wing, $\frac{p-p_\infty}{\frac{1}{2}\rho_a V_j^2 S}$
c	Chord length, ft (m)
D	Vehicle drag, lb (N)
D_w	Wave drag, lb (N)
d_a	Air drag, lb(N)
d_f	Form drag, lb (N)
d_w	Hydrodynamic drag, lb (N)
F	Froude number, $V/\sqrt{gc}$
f(h)	Cruise height function

g Gravitational constant, ft/sec^2 (m/sec^2)

H Height of wing above water, ft (m)

h Cruise height, ft (m)

h_w Wave height, ft (m)

L Lift, lb (N)

ℓ Characteristic length = chord, ft (m)

m Wave drag hump factor

$\dot{m}_f$ Forward mass flow rate = $A_f \rho_a V_j$

$\dot{m}_j$ Mass flow rate of fans = $A_j \rho_a V_j$

$\dot{m}_{te}$ Mass flow rate from under wing trailing edge = $A_{te} \rho_a V_j$

$\dot{m}_s$ Mass flow rate from under sidewalls = $A_s \rho_a V_{cr}$

n Wave drag curve slope

p Local static pressure, lb/ft^2 (N/m^2)

p_∞ Free stream static pressure, lb/ft^2 (N/m^2)

S Wing planform area, ft^2 (m^2)

T Thrust, lb (N)

V_{cr} Critical velocity = $V_j - V_a^2$, ft/sec (m/sec)

V_j Jet velocity, ft/sec (m/sec)

V_u Velocity under the wing, ft/sec (m/sec)

V_∞ Free stream velocity, ft/sec (m/sec)

W Vehicle weight, lb (N)

WT Vehicle density = $(W/S^{3/2})$ $(1/\rho_w g)$

ρ_a Density of air, lb/ft^3 (N/m^3)

ρ_w Density of sea water, lb/ft^3 (N/m^3)

ABSTRACT

Recent efforts in theoretical analysis and experimental observations have moved the concept of power-augmented flight in ground effect toward practicality. With the addition of lift and drag due to external airflow, end plate leakage, water skin friction, wave drag effects, and wave clearance constraints, a flow model can be made capable of effective comparison of different vehicle configurations in various operating environments. The analysis shows that there are wave drag and wave clearance related limits to many aspects of the vehicle configuration. The most important of these are cruising height and aspect ratio, in that they have a very large effect on transport efficiency. Unfortunately, the low flying high aspect ratio cases are ruled out due to wave impact problems. Testing of a point design vehicle, arrived at through the use of an analysis such as the one of this report, needs to be performed as final verification of the accuracy of the design procedure.

ADMINISTRATIVE INFORMATION

This report supports the Advanced Naval Vehicle Concept Evaluation (ANVCE) conducted by the ANVCE Project Office (NOP-96V). The Aviation and Surface Effects Department (ASED) of the David W. Taylor Naval Ship Research and Development Center (DTNSRDC) did the work. The Naval Air Development Center (NADC) funded the effort under Task Area SSH15002 with Project Order N62269/77/PO/00568. The DTNSRDC Work Unit Number was 1612-009.

INTRODUCTION

Inherent in the development of any class of vehicle is the need to predict their performance characteristics. Only recently has there been the necessary development of theory (Ref 1-2) and substantiating experiments on power-augmented ram wings to allow this.* With the addition of appropriate wave-drag factors derived from References 6 and 7 and constraints on such things as wave clearance and minimum C_L requirements, a vehicle analysis program has been generated.

---

*Reported informally by F. Krause ("Static Performance of a Power-Augmented Ram Wing," DTNSRDC ASED TM-16-76-74, May 1976; and "Parametric Investigation of a Power-Augmented Ram Wing Over Water," DTNSRDC ASED TM-16-76-95, Oct 1976).

The computer program described in this report has the capability of investigating a large number of vehicles of varying configurations operating in a variety of environments. It can also investigate the off-design performance of any configuration that proves promising.

THEORY

FLOW MODEL

External flow effects, end-plate leakage, end-plate wetting drag, propulsor scrubbing drag, and pressure patch hydrodynamic wave drag are added to the 2-D static Power-Augmented Ram Wing (PAR) flow models of References 1 and 2. These earlier models were corroborated by 2-D experiments for geometries giving high performance. Also, the basic mass, momentum, and energy balances on which the static theory rests are as valid in 3-D as for the 2-D case used in the original derivation. This 3-D validity has been corroborated experimentally.*

The external flow effects amount to additional lift and drag proportional to the free-stream dynamic pressure. These forces are calculated by assigning constant external lift and drag coefficients. Presumably, these coefficients can be bounded within suitably narrow ranges allowing concentration on the PAR features of the design.

End-plate leakage detracts from performance by allowing the air to escape from the cushion in a direction not parallel to the free-stream flow. This is basically the same mechanism as thrust loss due to divergence in conical rocket nozzles. As the air passes under the end plates, it is assumed to accelerate laterally only and to retain the same streamwise component of velocity it had under the wing. This model essentially requires separation and the concomitant shedding of a vortex sheet at the bottom of the end-plate. Since both of these phenomena have been observed experimentally on unaugmented ram wings (Ref 3), there is no reason to suppose that they would not occur here.

---

*Ibid., p.2.

The drag of the end-plates cutting through the tops of water waves is calculated by assigning a turbulent skin friction coefficient and multiplying by the wetted area and the dynamic pressure of the water. Certain empirical data (Ref 4) and test data (Ref 5) suggest that wetting drag could be much less at high speeds. End-plates with higher drag characteristics could also be constructed. These refinements however, are ignored. End-plate hydrodynamic lift is also neglected.

Wave drag is calculated from a curve fit to the Newman and Poole (Ref 6) analytical results. Subsequent calculations by Doctors (Ref 7) indicated that lower wave drag through hump is likely due to the gradual pressure changes at the leading and trailing edges in the real case, compared to the abrupt pressure changes assumed by Newman and Poole. This refinement, however, is inconsequential at the high cruise speeds of the PAR wing-in-ground effect (WIG) vehicle.

In summary, the momentum fluxes described in Figure 1 are summed to calculate the net thrust on the system. The various momentum fluxes at the leading edge are related by the previously developed 2-D solutions. The flow under the end-plates and trailing edge flap is modeled as a simple one-dimensional flow. In equilibrium, the resulting lift is equal to the constant pressure acting on the bottom of the wing times the wing area, plus the aerodynamic lift due to the external flow.

The power required by the system is the "air power" of the propulsor, defined as the mechanical energy flux through the propulsor exit minus the mechanical energy flux into the propulsor inlet.

ANALYSIS AND DERIVATIONS

The theory used in this analysis was based on the work of Gallington and Chaplin (Ref 1 and 2). The resulting equations of primary importance to this study are (Figure 1):

$$T = \underbrace{-\dot{m}_f V_j}_{\text{Thrust Reversal Component}} + \underbrace{\dot{m}_f\sqrt{V_j^2 - V_{cr}^2}}_{\text{Sidewall Leakage Component}} + \underbrace{\dot{m}_{te} V_j}_{\text{Trailing Edge Exhaust Component}} - \underbrace{\dot{m}_j V_\infty}_{\text{Fan Ram Drag}} \quad (1)$$

$$D = \underbrace{\tfrac{1}{2}\rho_w V_\infty^2 C_f A_w}_{\text{Sidewall Water Drag}} + \underbrace{\tfrac{1}{2}\rho_a V_\infty C_{DP} S}_{\text{Form Drag Component}} + \underbrace{\tfrac{1}{2}\rho_a V_u^2 C_{fa} S}_{\text{Power Augmentation Drag Under Wing}} \quad (2)$$

$$L = W = \underbrace{\tfrac{1}{2}\rho_a V_j^2 C_p S}_{\left(\begin{array}{c}\text{Power Augmentation}\\ \text{Lift Component}\end{array}\right)} + \underbrace{\tfrac{1}{2}\rho_a V_\infty^2 C_L S}_{\left(\begin{array}{c}\text{Airfoil Lift}\\ \text{Component}\end{array}\right)} \tag{3}$$

Setting thrust equal to drag and dividing by $A_j \rho_a V_j^2$ yields

$$-\frac{A_f}{A_j} + \frac{S}{A_j}\sqrt{C_p}\,(1-C_p)^{\frac{1}{2}} + \frac{A_{te}}{A_j} - \frac{V_\infty}{V_j} = \tfrac{1}{2}\frac{\rho_w}{\rho_a}\left(\frac{V_\infty}{V_j}\right)^2 C_f \frac{A_w}{A_J} + \tfrac{1}{2}C_{DP}\left(\frac{V_\infty}{V_j}\right)^2 \frac{S}{A_j}$$

$$+ \tfrac{1}{2}C_{fa}\left(\frac{V_u}{V_j}\right)^2 \frac{S}{A_j} + \frac{D_w}{A_j \rho_a V_j^2} \tag{4}$$

Note that a wave drag term has been added in Equation (4). This is derived from the work of Newman and Poole (Ref. 6) and is presented in Equation (5).

$$D_w = \frac{P}{\ell} L\,(AF^{-m} + BF^n)^{-1} \tag{5}$$

From the "filled-duct" potential flow solution derived in Reference 2, the following area ratios can be determined:

$$\frac{A_f}{A_j} = 1 - \frac{4(1 - C_p)^{\frac{1}{2}}}{[1+(1-C_p)^{\frac{1}{2}}]^2} \tag{6}$$

$$\frac{A_{te} + \sqrt{C_p}\,A_s}{A_j} = \frac{4(1-C_p)^{\frac{1}{2}}}{[1+(1-C_p)^{\frac{1}{2}}]^2} \tag{7}$$

$$\frac{A_{te}}{A_j} = \frac{4\,(1-C_p)^{\frac{1}{2}}}{[1+(1-C_p)^{\frac{1}{2}}]^2} - \sqrt{C_p}\,\frac{A_s}{A_j} \tag{8}$$

and then substituted into Equation (4) to get :

$$\frac{\text{Power}}{WV_\infty} = \frac{\left(\left(\frac{V_j}{V_\infty}\right)^2 - 1\right) \frac{V_j}{V_\infty} \frac{A_j}{S}}{\left(\frac{V_j}{V_\infty}\right)^2 C_p + C_L} \tag{9}$$

where

$$\frac{A_j}{S} = \frac{2\frac{\rho_w}{\rho_a}\left(\frac{V_\infty}{V_j}\right)^2 C_{fw}\frac{A_w}{S} + \tfrac{1}{2}C_{DP}\left(\frac{V_\infty}{V_j}\right)^2 + \tfrac{1}{2}C_{fa}(1-C_p)}{\frac{8(1-C_p)^{\frac{1}{2}}}{[1+(1-C_p)^{\frac{1}{2}}]^2} - 1 - \frac{V_\infty}{V_j}}$$

$$+ \frac{2\frac{A_s}{S}\sqrt{C_p}\,(1-\sqrt{1-C_p}) + \frac{D_w}{S\rho_a V_j^2}}{\frac{8(1-C_p)^{\frac{1}{2}}}{[1+(1-C_p)^{\frac{1}{2}}]^2} - 1 - \frac{V_\infty}{V_j}} \tag{10}$$

The inverse of Equation (9) is the transport efficiency, which is the primary point of comparison between one vehicle geometry and another. A unique feature of the computation procedure is the selection of the depth of end-plate clipping which results in the minimum effective drag. As the end-plate runs deeper in the water, air leakage under the end plate is reduced (a favorable effect) while the water drag increases (an unfavorable effect). Refer to Figure 2 and imagine the end plate being lifted by an amount dh in a wave of amplitude one. There is a reduction of water drag proportional to $4C_{fw}\tfrac{1}{2}\rho_w V_\infty^2 \cos^{-1}(h)dh$, and an increase in air

drag (or thrust reduction) of $2\rho_a V_{cr}(1-V_u)\cos^{-1}(h)dh$. The minimum effective drag resulting from this trade-off occurs when

$$f(h) = C_{fw}\frac{\rho_w}{\rho_a}\left(\frac{V_\infty}{V_j}\right)^2\cos^{-1}(h) - \sqrt{C_p}[1-(1-C_p)^{\frac{1}{2}}]\cos^{-1}(-h) = 0 \qquad (11)$$

This transcendental equation is solved for h by a Newton-Raphson iteration in the design procedure of the program (System I). In the analysis procedures (Systems II and III), h is specified and the Newton-Raphson procedure is not used.

The area available for side flow under the end plates A_s and the total wetted area of the end plates A_w are calculated from

$$\frac{A_s}{S} = \frac{1}{\pi}\frac{hw}{\sqrt{S}}\frac{1}{\sqrt{AR}}\{2h[\pi-\cos^{-1}(h)] + 2\sin[\cos^{-1}(h)]\} \qquad (12)$$

and

$$\frac{A_w}{S} = \frac{2}{\pi}\frac{hw}{\sqrt{S}}\frac{1}{\sqrt{AR}}\{2\sin[\cos^{-1}(h)] - 2h\cos^{-1}(h)\} \qquad (13)$$

The average size of the leakage areas under the side plate and the amount of water-wetted end plate surface area, as functions of the elevation of the bottom of the end plate with respect to mean sea level, are calculated by representing the design sea state with sinusoidal waves corresponding to the significant waves. The adequacy of this assumption may be assessed by computing, for the "statistically correct" sea state, the probability (averaged over time or distance) of encountering water at each elevation as a function of elevation, and comparing with a similar calculation for the assumed sinusoidal waves. Such a comparison is shown in Figure 3 for upper sea state 5. Both models show

the occurrence of air and water to be equally probable at mean sea level. The sinusoidal model fits well at large and small elevations and gives exactly the correct slope passing through mean sea level. Minor differences occur between 2 and 3 feet, and they are totally negligible in the calculation of drag-especially considering the other approximations that had to be made.

DESIGN PROCEDURE

SYSTEM I

This system is intended to examine the capabilities of a wide range of vehicle configurations and operating parameters in a given environment. That environment is defined by the relative wave height, wave clearance requirements (i.e., 1/3 highest, 1/1000 highest, etc.), and vehicle density, which is related to payload-range requirements.

For a given aspect ratio, the pressure coefficient under the wing (C_p) is varied from 0.1 to 0.9, while the ratio V_∞/V_j is varied over the same range. Variations in C_p are related to changes in the trailing edge gap (and therefore the flap angle), while the changes in V_∞/V_j correspond to different engine operating conditions. At each pair of C_p and V_∞/V_j points, the optimum performance (or minimum drag) case is calculated for comparison with the other operating cases for the same aspect ratio. Not all operating cases are available for comparison, however, because certain constraints (discussed below) might not be satisfied. Of the remaining operating cases, the one with the best transport efficiency is chosen as the best case for that aspect ratio (under the constraints of the specified environment.)

Some computed operating points are impractical because of two possible limitations: First, it is difficult to stabilize an unaugmented wing in ground effect at very low lift coefficients because the lift becomes more weakly dependent on ground clearance. The PAR-WIG eventually becomes unaugmented at the higher speeds where the jet velocity and the free-stream velocity are not much different. Therefore, it seems appropriate

to specify a lower limit to the permissible lift coefficient. This lift coefficient limit can also be used as a correctly-scaled structural integrity speed limit. Second, while the drag is calculated using an average sinusoidal wave, there are larger waves in the design sea state, and the bottom of the wing must clear these larger waves. Therefore, we reject designs in which the filled duct solution indicates a wing height less than a certain factor times the design wave height. Typically, the drag calculation is based on sinusoidal waves of amplitude equal to the significant wave height of the design sea state, and the wing bottom is required to clear a wave of twice the significant wave height (or the largest wave expected in 1000 wave encounters). Alternatively, the drag can be based on the average wave height, and the wing bottom can be required to clear a wave of three times the average wave (again the largest wave expected in 1000 wave encounters).

This process is carried out for a range of aspect ratios. It is therefore possible to compare a vast number of vehicles operating in a variety of environments. The configurations that appear to be the most promising are then examined in SYSTEM II and SYSTEM III for their off-design performance.

OFF-DESIGN PERFORMANCE

Having selected the major parameters, using the design procedure described above, the next step is to predict how that particular craft will perform at off-design conditions. There are two off-design conditions of primary interest. First, one may want to accelerate as fast as possible from rest to the cruise condition in the design (or lower) sea state by keeping the side plates at a depth which results in minimum effective drag (System II). The second important off-design condition is operation at an arbitrary height either to decelerate by dropping the end plates in the water or to clear a given wave condition with the bottom of the wing (System III). A corollary possibility is to predict the performance of a given configuration over smooth water at a given height (or end plate depth).

SYSTEM II - EXCESS THRUST WITH END PLATES AT OPTIMUM DEPTH

For each given C_p and V_∞/V_j, the calculation of the ideal jet area for the filled duct proceeds exactly as before. For off-design conditions, however, one cannot change the engine exit area at will. The difference between the ideal jet area and the installed jet area represents an excess thrust or drag, depending on which is larger. There is excess thrust if the installed jet area is larger than the optimum jet area. For the purpose of this calculation, we assume that the momentum flux associated with the excess installed jet area compared to the jet area required by the filled duct solution appears as excess thrust. This excess thrust is then used to compute the acceleration. There is an underlying assumption that the theoretical filled duct performance is achieved for the calculated (required) jet area. In Figure 2, a comparison is made between the design flow model and the off-design flow model.

SYSTEM III - PERFORMANCE AT ARBITRARY HEIGHT

In System III, the acceleration or deceleration of the craft operating at a height different from that which would result in minimum drag is predicted. The calculation procedure is exactly as in System II, except that the end-plate wave cutting depth is not optimized for minimum drag; instead, the wave cutting depth is set at some specific value. Again, the required jet area for the filled duct solution is computed. If the installed jet area exceeds the calculated jet area, the excess thrust is calculated exactly as in System II (see Figure 4).

RESULTS

To generate output suitable for discussion, we arbitrarily assign the following constant values:

Lift Coefficient of External Flow	C_{LU}	= 0.3
Turbulent Air Skin Friction	C_{fa}	= 0.003
Turbulent Water Skin Friction	C_{fw}	= 0.0003

Drag Coefficient of External Flow	C_{DP}	= 0.04
Minimum Cruise Lift Coefficient	C_{Lmin}	= 1.5
Minimum Wing Clearance	$\frac{H}{h_w}$	= 2 ($h_{1/3}$, used for drag)
	$\frac{H}{h_w}$	= 3 (h_{AVE}, used for drag)

GENERAL TRENDS

All of the results presented represent the best performance conditions available for the parameters specified, including wave clearance and C_L limits.

An increase in aspect ratio results in a general increase in the transport efficiency regardless of changes in other parameters (see Figures 5, 7 and 9). Conversely, as aspect ratio increases, the Froude number based on $\sqrt{S}$ decreases to a greater or lesser degree; see Figures 6, 8, and 10. Again, this general trend is evident regardless of the variation of other parameters such as wave clearance, vehicle density, and relative wave height. The wave clearance constraints, which are checked at each discrete point on the C_p versus V_∞/V_j map, accounts for the irregular (almost quantum) jumps in these curves. This is because an increase in aspect ratio results in a decrease in the cruise height, since the frontal area (defined by span x cruise height) is held constant. At some point, this cruise height will be less than the specified wave clearance, and it will be ruled out as a possible operating condition.

As can be seen in Figure 5, the transport efficiency increases with decreasing relative wave height. This is because the WIG can cruise closer to the surface with less interference from wave impact. Figure 6, however, shows that the Froude number decreases with decreasing relative wave height. The reduction in best Froude numbers (based on $\sqrt{S}$) in smaller waves is probably due to a reduction in thrust loss under the end plates, allowing a lower efficient cruise speed as compared to that in higher waves.

Vehicle density has virtually no effect on transport efficiency (Figure 7), but it has a clear effect on the Froude number. Figure 8 shows an increase of 20 to 30-percent in the Froude number when the density of the vehicle is doubled.

Only a 10- to 25-percent increase in transport efficiency was achieved when the wave clearance constraint was relaxed by 50-percent (Figure 9). The effect of that same change in the clearance constraint on the Froude number was mixed and showed some dependence on aspect ratio (Figure 10). Above an aspect ratio of 2.0, the lower wave clearance allows a lower Fourde number (e.g., a lower cruise velocity and cruise height), and therefore a higher transport efficiency. For aspect ratios less than 2.0, the reverse appears to be the case; however, the trend is not sustained enough to allow great confidence in that conclusion.

EXAMPLE OF OFF-DESIGN PERFORMANCE CALCULATION

Figure 11 illustrates the calculations of off-design performance of a given power-augmented WIG. The performance of the PAR feature at forward speed is represented by the superposition of lines of constant C_p, constant V_∞/V_j, and constant Froude number. These three families of lines can be constructed from the computer output of System II for the minimum drag assumption or from System III for the constant height assumption. A "vehicle characteristic" can also be constructed passing through all trim points (T = D, no longitudinal acceleration) in any sea state. The vehicle characteristic for the design sea state passes through the design point D. The off-design vehicle characteristics are obtained by running System II or III for the given vehicle in the new sea state. The propulsion system has a characteristic variation of jet velocity V_j with forward speed (i.e., Froude No.); this propulsion characteristic for the design case engine operating at design power passes through the design point. High power settings or low power settings are represented by other, roughly parallel, characteristics.

To illustrate the computation of off-design performance, consider

the possibility of variations away from the design point D in Figure 11. As power is increased at constant speed, the operating point moves along a constant Froude number line to the new power characteristic, i.e., point A. Note that V_j increases and C_p decreases in the process while V_∞ remains constant. The vehicle then accelerates, according to the values given in the computer output as a function of C_p and V_∞/V_j, along the new power characteristic to point B where the speed (Froude No.) is higher. A deceleration resulting from a power reduction occurs in a converse way moving first from D to C and then to E.

Another possibility is operation at other than the design sea state. If the existing sea state is less than the design case and constant power is maintained, the craft accelerates (according to the values from the output of System II or III for the reduced sea state) along the propulsion characteristic to point F. Conversely, if the sea state increases, the vehicle decelerates to G along the propulsion characteristic by a similar process. Another possibility is to reduce power and maintain speed in the smaller waves thus moving to point C. The transport efficiency at F is generally better than at C; this suggests that the higher speed, rather than the reduced power cruise, is preferred in the low sea state.

COMPUTER PROGRAM

The performance analysis program consists of a main program segment, three primary subroutines, and six subordinate subroutines. The main program does little more than read in the data and control the use of the three primary subroutines based on a set of commands (also input as data).

Primary subroutine one (SYSTEM I in Figure 12) assumes the filled duct solution of the momentum flux model and unrestricted cruise height operation. The subroutine then calculates the Froude number, cruise height, transport efficiency (including wave drag effects), and checks for wave clearance and C_L minimums by calling FROUDE, HEIGHT, TRANS, and CHECK, respectively; see Figure 12. This is done for a range of C_p and

V_∞/V_j values; the results are then sent to "MAP" (see Table 1 for sample of MAP). This procedure is carried out for each of the aspect ratio cases specified by the input data to the main program segment.

Primary subroutine two (SYSTEM II in Figure 12) uses a predetermined aspect ratio and A_j/S ratio in conjunction with an essentially fixed end-plate size. SYSTEM II compares the performance characteristics of the minimum drag case (for a given C_p, V_∞/V_j pair) with those of the design point. The result is presented in terms of vehicle excess power (non-dimensionalized by WV), and vehicle acceleration in g's. Subroutines HEIGHT, CHECK, and FROUDE are utilized, as well as MAP and MAPB which generates the "Acceleration Map." (See Table 2 for sample of MAPB.) Control is then returned to the main program.

Primary subroutine three (SYSTEM III in Figure 12) operates in the same way as does SYSTEM II. SYSTEM III, however, uses a fixed cruise height instead of a calculated height based on minimum drag. It, therefore, calls only FROUDE and CHECK along with generating the outputs of MAP and MAPB.

The first of the six subordinate subroutines is HEIGHT. This routine performs a Newton-Raphson iteration of Equation (11) and returns the minimum drag cruise height. This height is an end-plate emersion factor that corresponds to a balance between hydrodynamic drag and loss of entrapped air from under the end-plate.

Subroutine FROUDE calculates the Froude number (as a function of chord) for each pair of C_p and V_∞/V_j points to be presented on the map.

The transport efficiency is calculated by subroutine TRANS and is based on Equations (9) and (10) of the "filled duct" momentum flux model presented earlier.

CHECK performs a simple comparison between the cruise height and the combination of wave height and wave clearance factor. It also checks to see if the vehicle's cruise C_L is above a prescribed minimum. Appropriate flags are included on the efficiency map at each collocation point.

Subroutine MAP presents the results of the design performance analysis as numerical values at their corresponding collocation points. Each group of values is presented in the following order: (from top to bottom) transport efficiency, cruise height factor, cruise height and C_L limit flags (if any), and Froude number (see Table 1).

Subroutine MAPB presents the results of the off-design performance analysis as numerical values at their corresponding collocation points. The values presented at each point are: height of wing lower surface above mean sea level (divided by $\sqrt{S}$), vehicle acceleration (in g's), and P/WV (again in order from top to bottom in Table 2).

CONCLUSIONS

A computer program was generated to evaluate the performance characteristics of power-augmented ram wing vehicles. The program was based on an amalgam of theoretical and experimental investigations regarding PAR flow phenomena and wave drag behavior. Off-design behavior of selected configurations can also be evaluated in a variety of operating environments. With the aid of this computer program some important conclusions can be drawn.

o The effects of increasing aspect ratio are to increase the transport efficiency and decrease the Froude number (based on $\sqrt{S}$). This, however, results in a decrease in the cruise height, and is subject to wave impact constraints.

o Vehicle density seems only to affect Froude number (in a direct way), while leaving the transport efficiency essentially unchanged.

o A decrease in relative wave height results in an increase in the transport efficiency; cruise height is reduced and there is less flow from under the end plates.

o The results of the program analysis seem reliable enough to warrant the logical next step of any design procedure. That next step should be to choose a promising design and compare the predicted performance with that of a test vehicle (probably a fully articulate model).

REFERENCES

1. Gallington, R. W., "Sudden Deceleration of a Free Jet at the Entrance to a Channel," DTNSRDC Report ASED 350 (Jan 1976).

2. Gallington, R. W. and H. R. Chaplin, "Theory of Power Augmented Ram Lift at Zero Forward Speed," DTNSRDC Report ASED 365 (Feb 1976).

3. Gallington, W. W., "Vortex Shedding from the Ram Wing Vehicle," Paper presented to the International Hovering Craft, Hydrofoil and Advanced Transit Systems Conference, Brighton, England (May 13-16, 1974).

4. Van Dyck, R. L., "Final Engineering Report on the Wake Shapes of Planing Forms Associated with High Speed Waterbased Aircraft," Stevens Institute of Technology Report 768, U020701 (Oct 1960).

5. Barkley, W. B., "Force and Spray Characteristics of Wing End Plates Penetrating the Water Surface," General Dynamics/Convair Report GD/C-64-100 (Apr 1964).

6. Newman, J. N. and F. A. P. Poole, "The Wave Resistance of a Moving Pressure Distribution in a Canal," Schiffstechnik, Vol. 9 (1962).

7. Doctors, L. J., "The Experimental Wave Resistance of an Accelerating Two-Dimensional Pressure Distribution," Journal of Fluid Mechanics Vol. 72, Part 3 (Dec 1975).

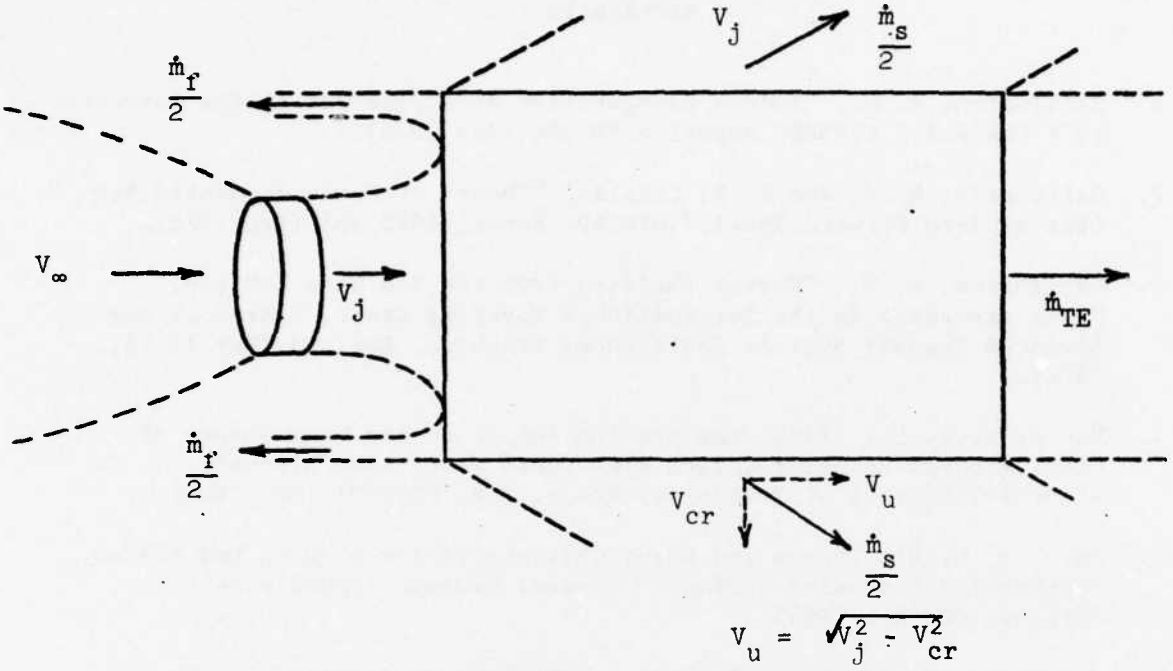

Figure 1a - Top View

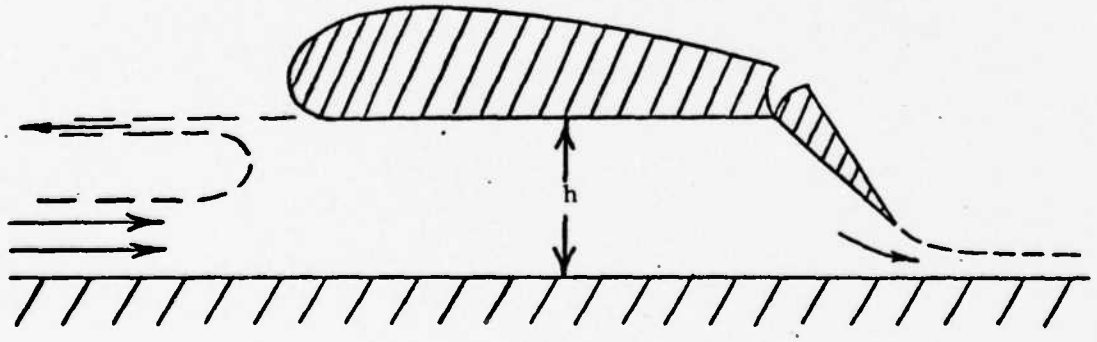

Figure 1b - Side View

Figure 1 - Momentum Flux Model

SYSTEM II

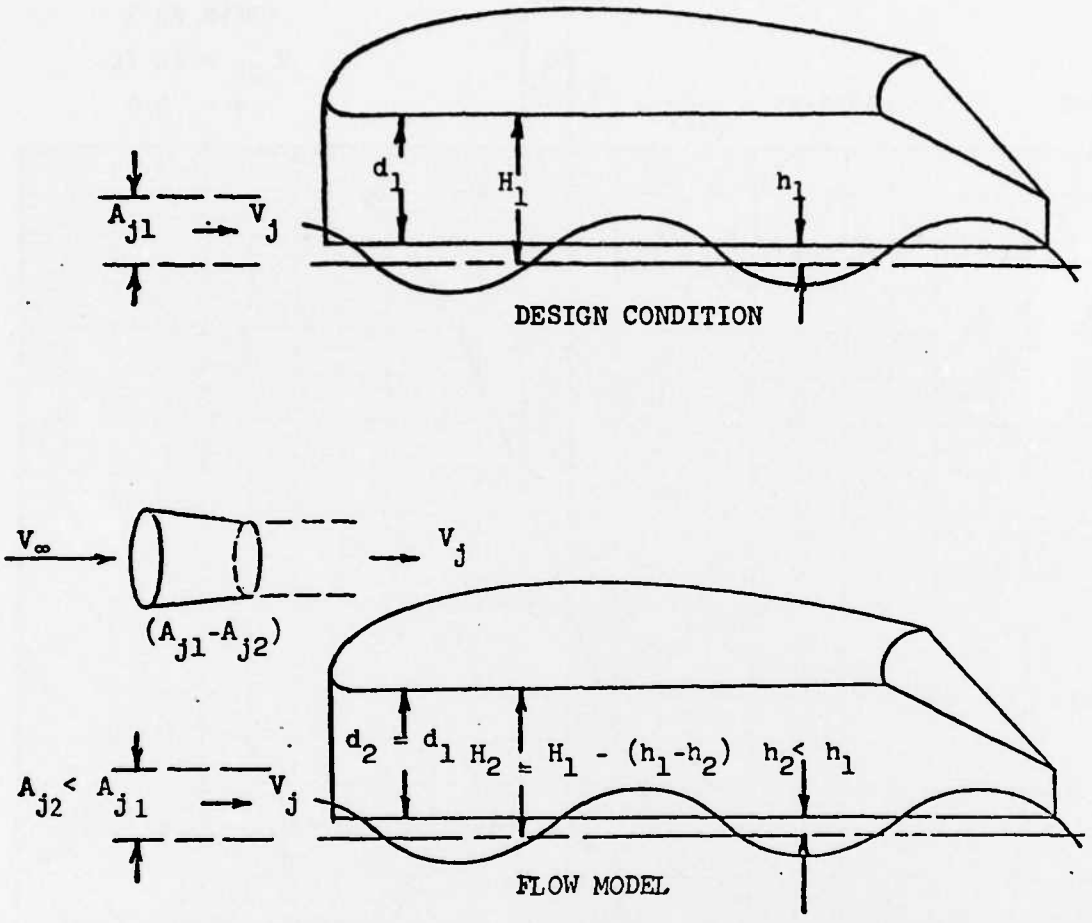

BELOW DESIGN SPEED

Figure 2 - Off-Design for Maximum Acceleration

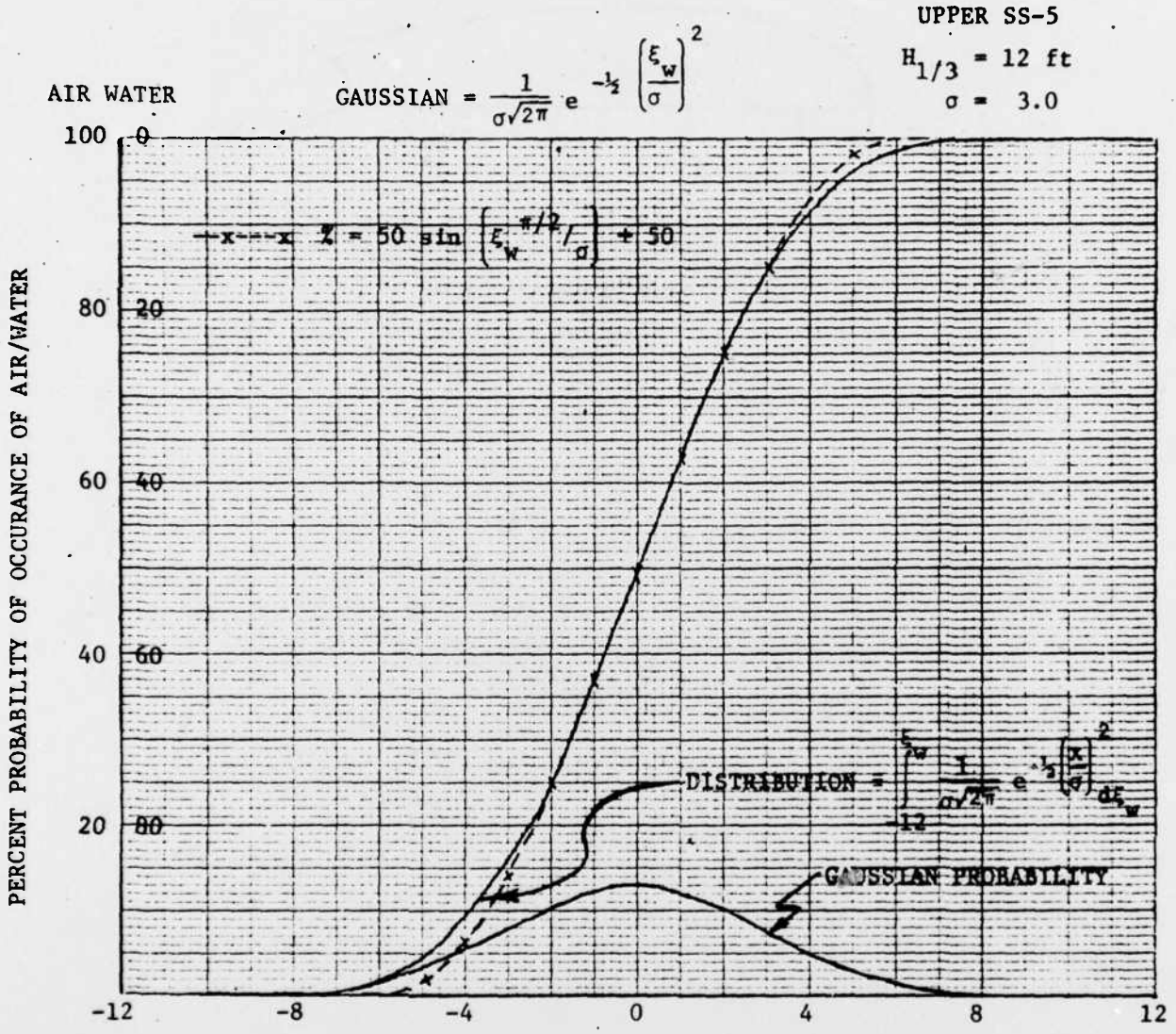

Figure 3 - Comparison of Modeled and Actual Wave Encounter Probabilities

SYSTEM III

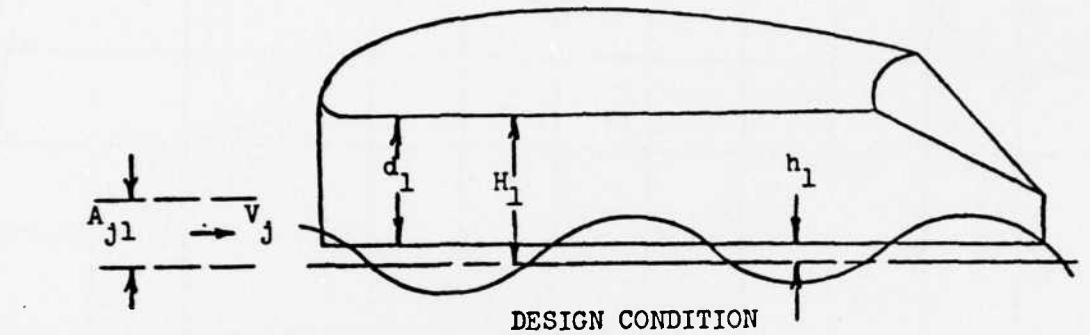

DESIGN CONDITION

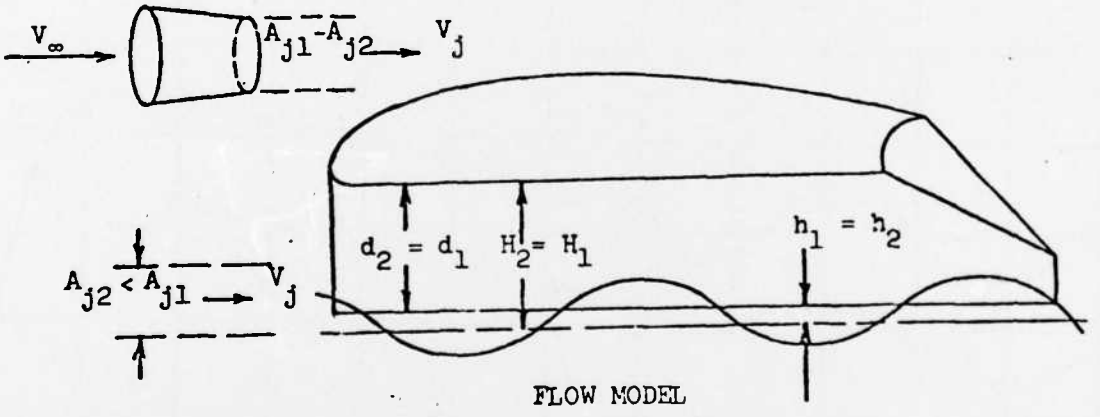

FLOW MODEL

BELOW DESIGN SPEED

Figure 4 - Off-Design at Constant Height

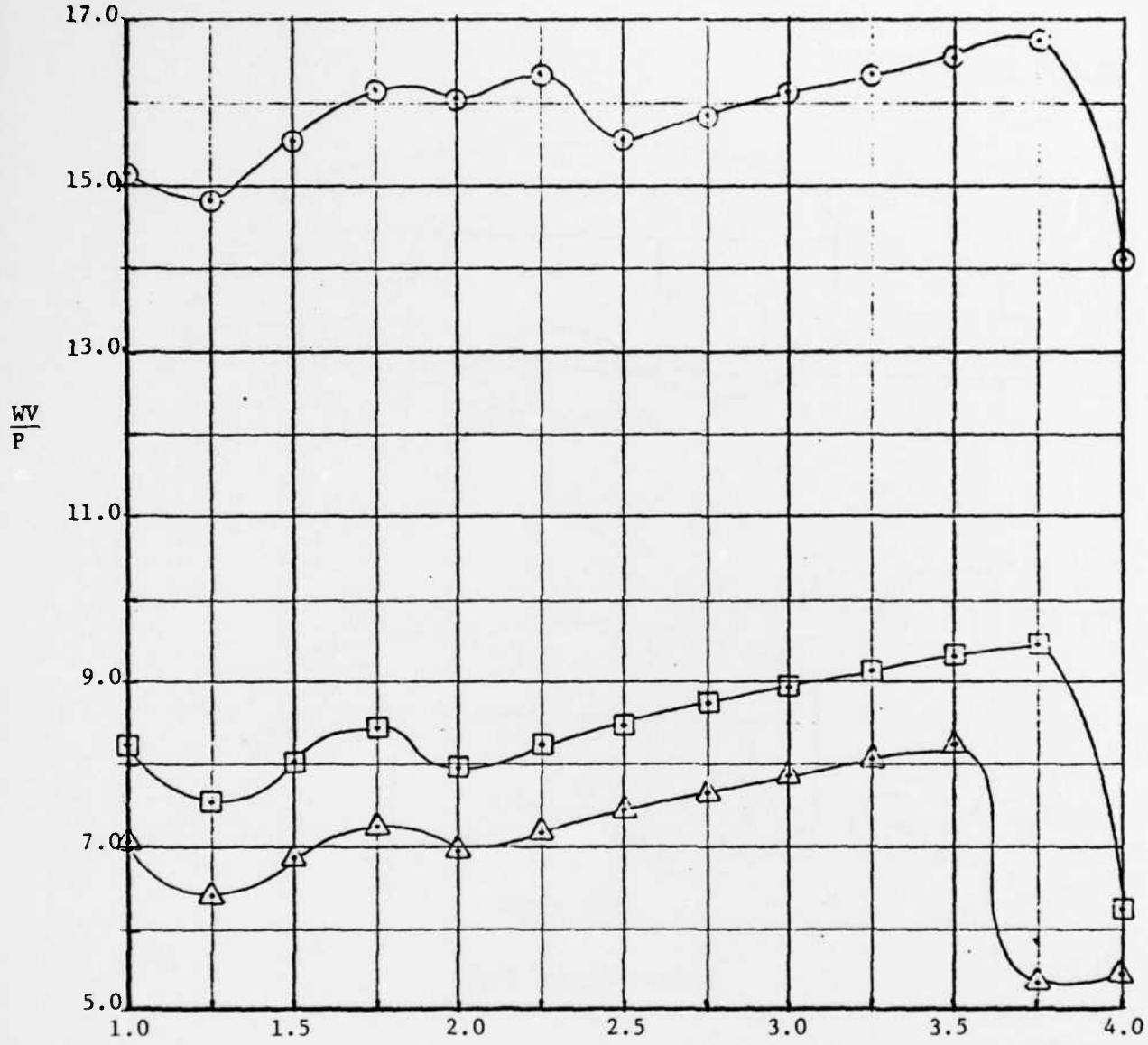

$\frac{h_w}{\sqrt{S}}$ $\frac{H}{h_w} > 2$ WT = 1/30

0.015 ○

0.04 □

0.05 △

Figure 5 - Effects of Relative Wave Height on Transport Efficiency as a Function of Aspect Ratio

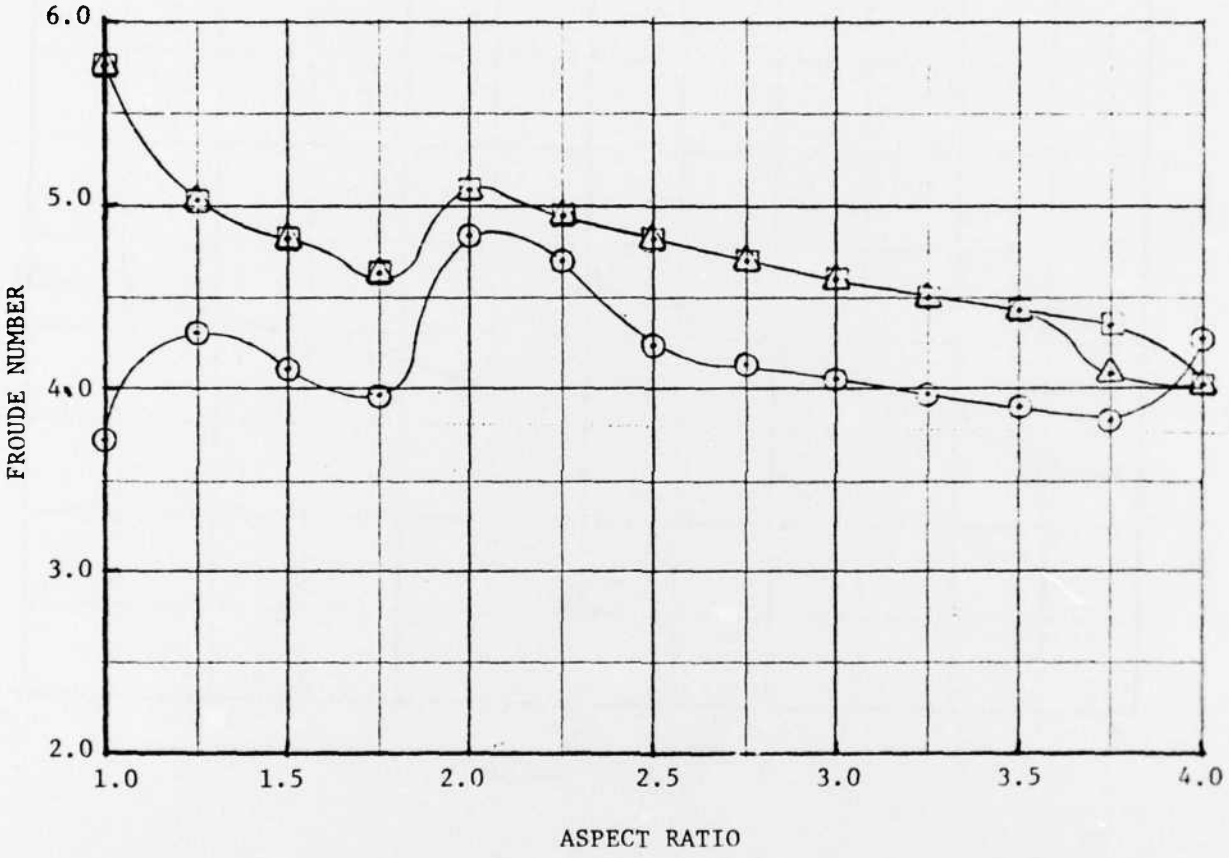

$\frac{h_w}{\sqrt{S}}$

0.015 ○

0.04 ⊡

0.05 △

$\frac{H}{h_w} > 2$

WT = 1/30

Figure 6 - Effects of Relative Wave Heights on Froude Number as a Function of Aspect Ratio

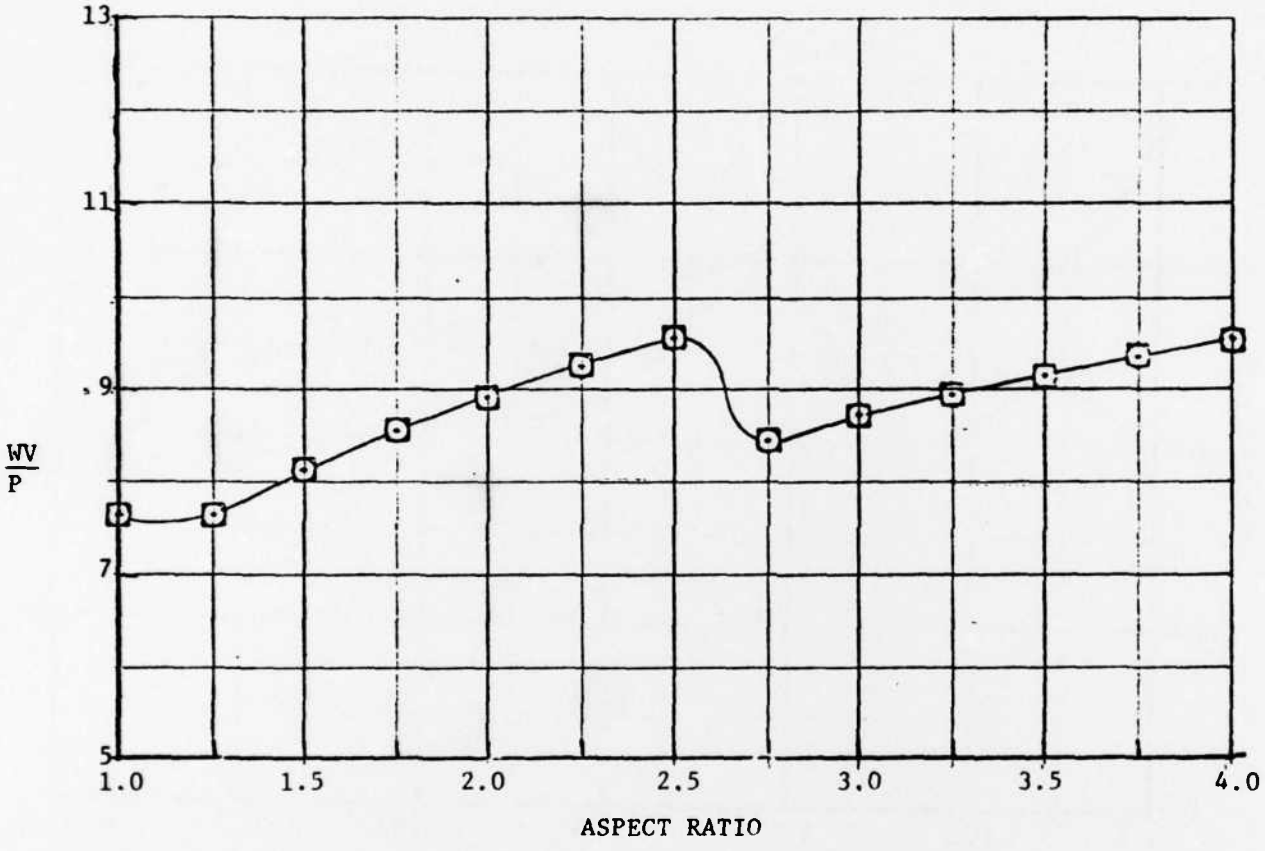

WT

1/30 ⊙

1/60 ⊡

$\frac{h_w}{\sqrt{S}} = 0.05$ $\frac{H}{h_w} > 1$

Figure 7 - Effects of Vehicle Density on Transport Efficiency as a Function of Aspect Ratio

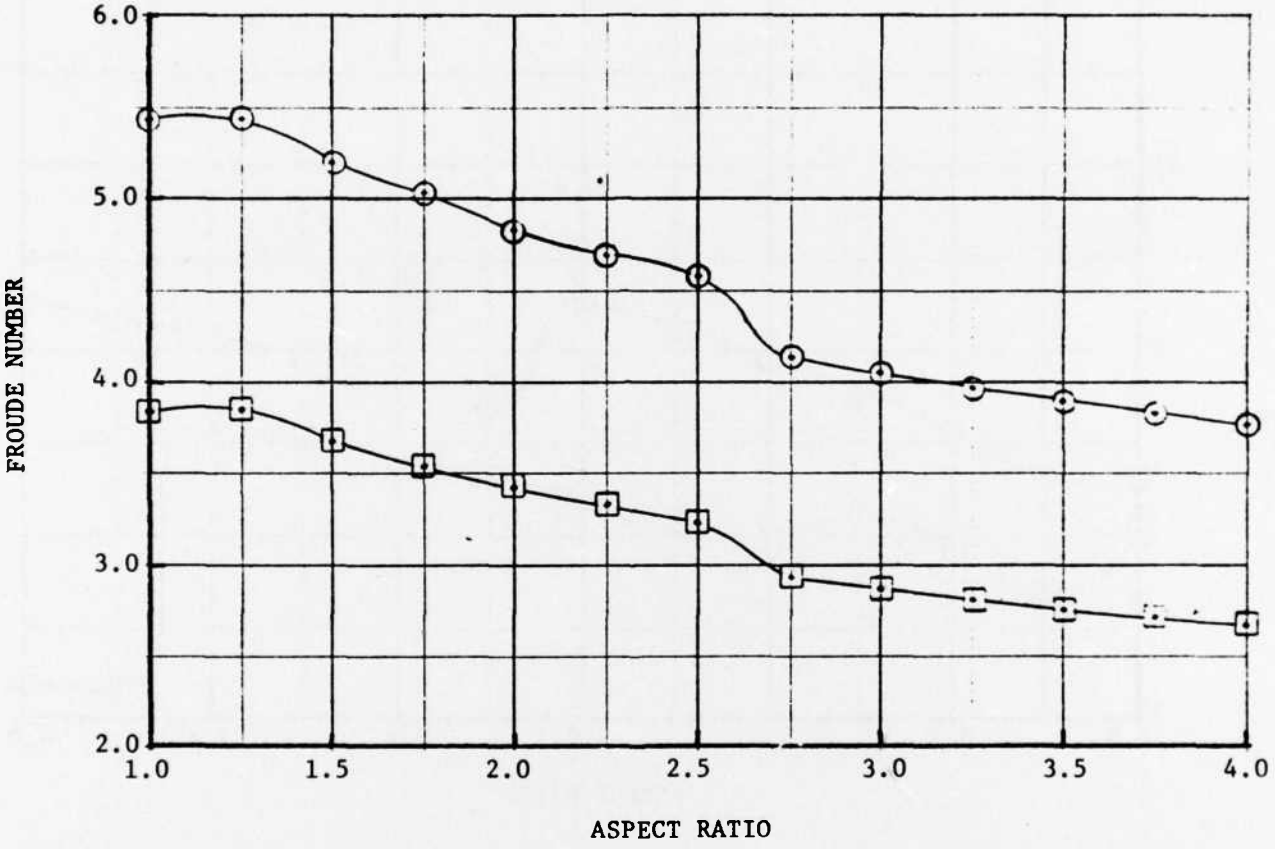

$\frac{WT}{1/30}$ ⊙ $\qquad \frac{h_w}{\sqrt{S}} = 0.05 \qquad \frac{H}{h_w} > 1$

1/60 ⊡

Figure 8 - Effects of Vehicle Density on Froude Number as a Function of Aspect Ratio

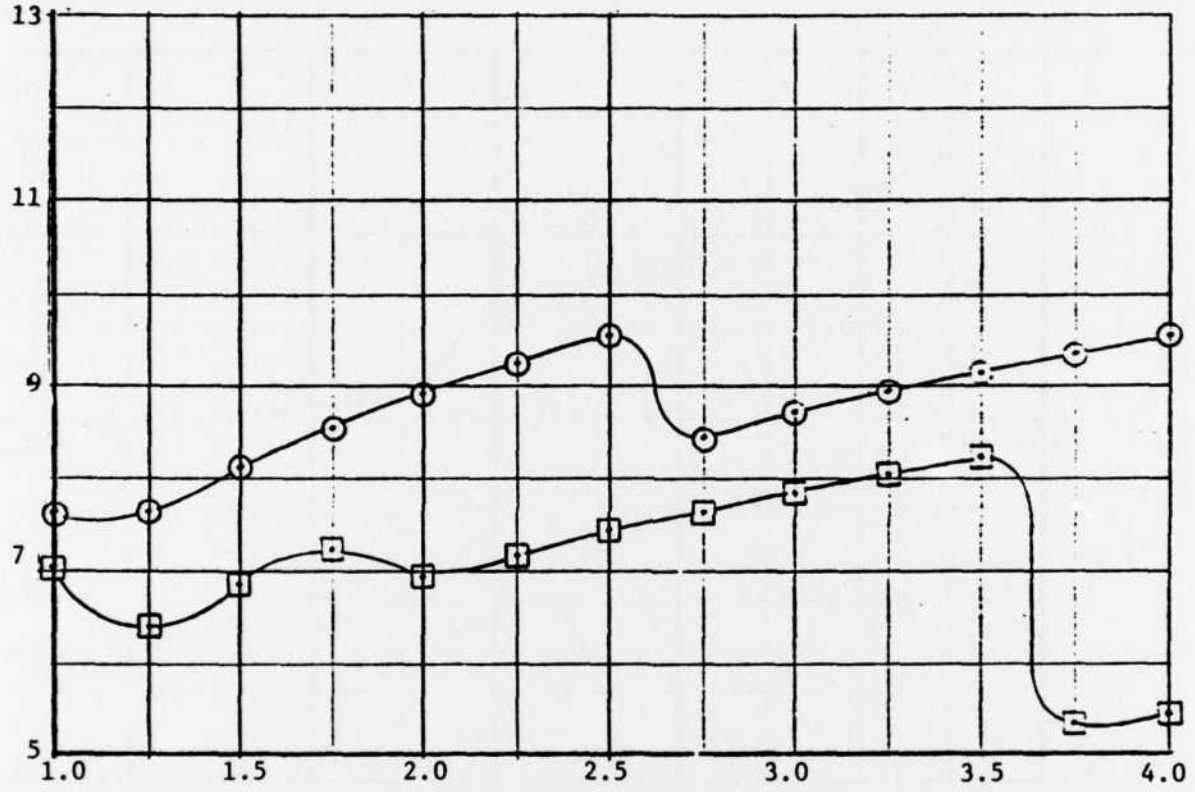

⊡ $\frac{H}{h_w} > 1$ $\frac{h_w}{\sqrt{S}} = 0.05$ WT = 1/30

⊙ $\frac{H}{h_w} > 2$

Figure 9 - Effects of Wave Clearance Constraints on Transport Efficiency as a Function of Aspect Ratio

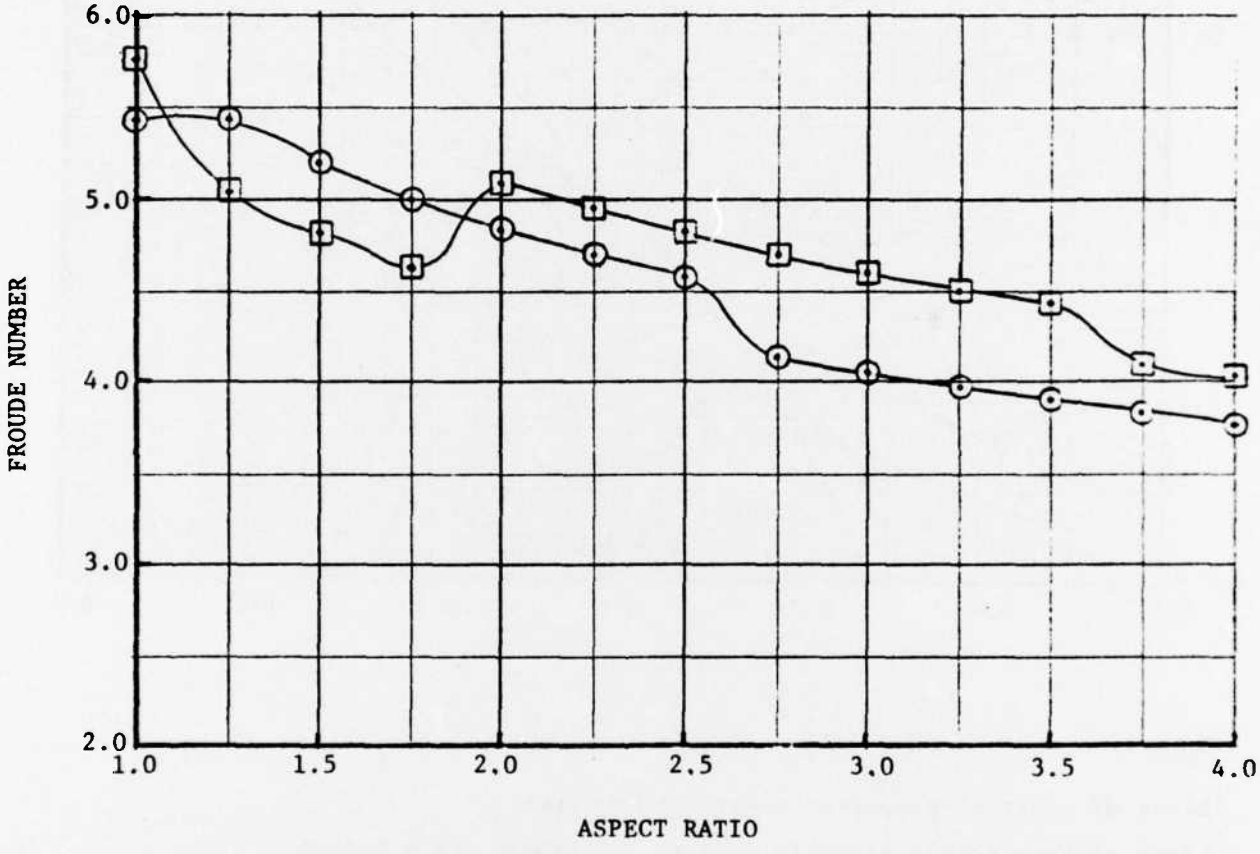

Figure 10 - Effects of Wave Clearance Constraint on Froude Number as a Function of Aspect Ratio

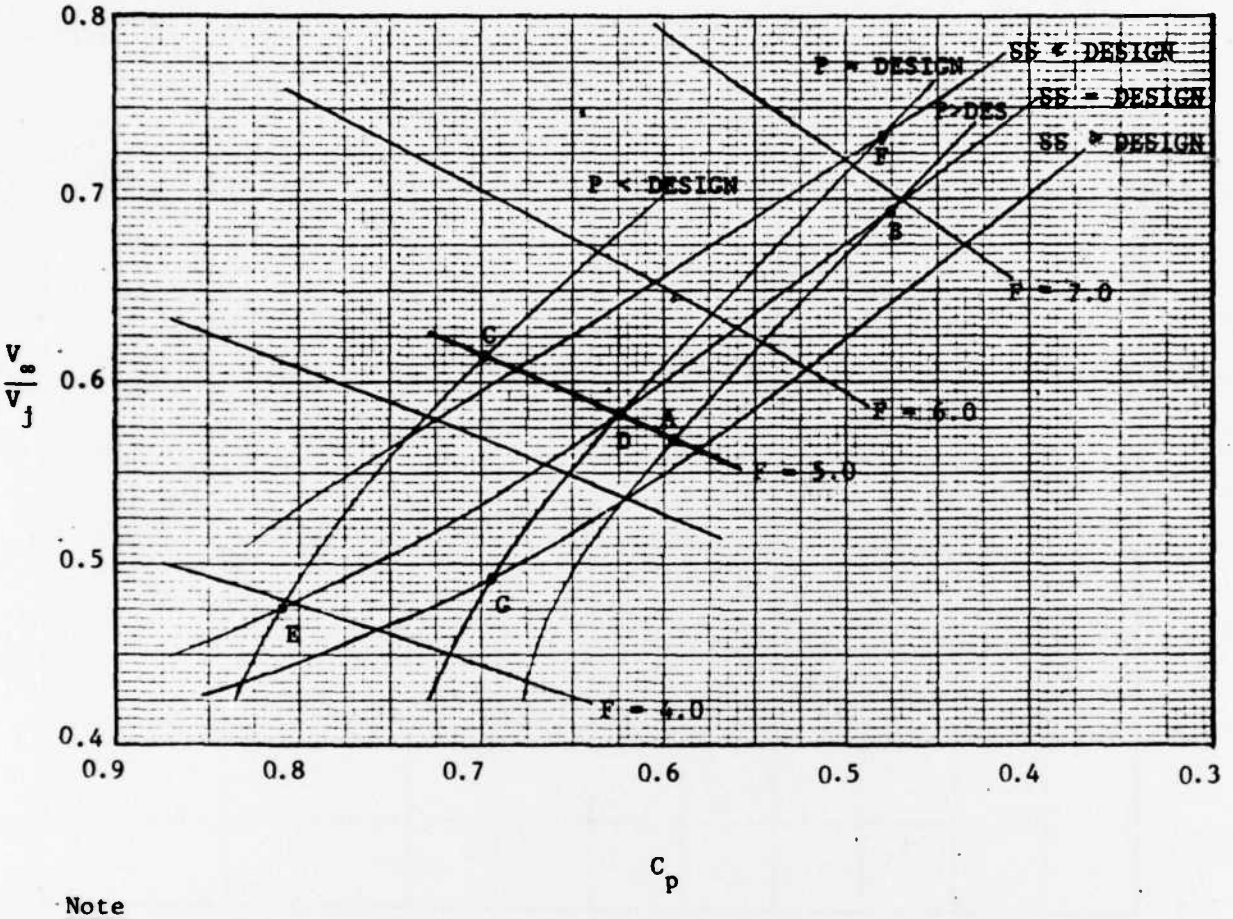

Note

Lines of constant propulsor power: $P \lessgtr$ Design

Lines of zero acceleration in a given sea state: $SS \lessgtr$ Design

Lines of constant Froude Number: F = 0.0

Figure 11 - Off-Design Performance

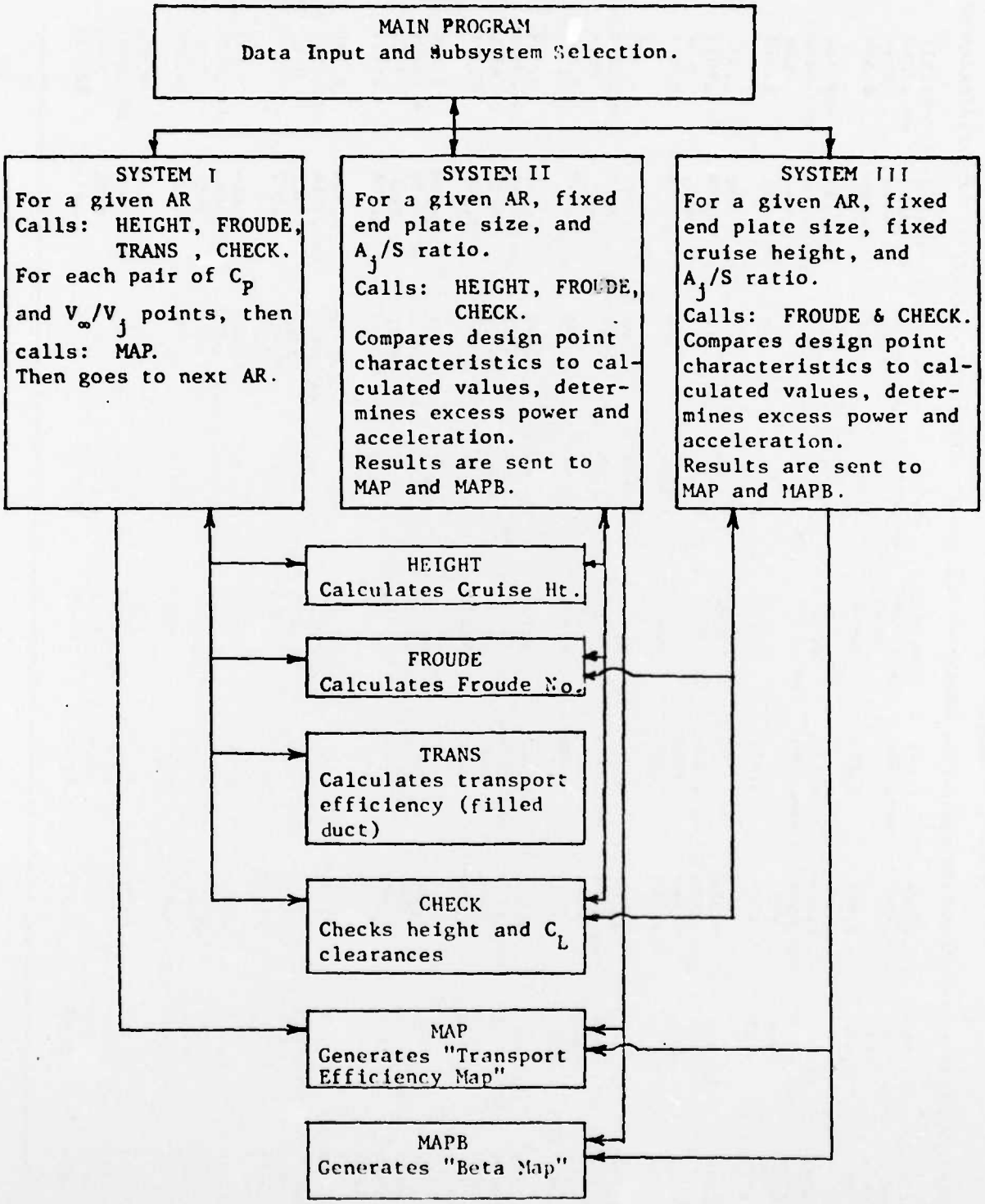

Figure 12 - Performance Program Format

TABLE 1 - SAMPLE TRANSPORT EFFICIENCY MAP

P.A.R.W.I.G. TRANSPORT EFFICIENCY MAP

CP									
	13.398	6.032	2.924	1.041	-.743	-3.131	-7.107	-15.260	-40.237
.9	H=-.9431	H=-.6121	H=-.3867	H=-.3584	H=-.0229	H= .2381	H= .4696	H= .6207	H= .7265
	***H	***H			***H	***H	***H	***H	CL.H
	.826	1.644	2.444	3.223	3.972	4.688	5.367	6.006	6.604
	14.260	10.489	6.915	5.174	3.931	2.219	.257	-4.407	-18.848
.8	H=-.9454	H=-.8618	H=-.5504	H=-.1594	H= .1883	H= .4463	H= .6238	H= .7404	H= .8182
	***H	***H	***H					***H	CL.H
	.875	1.741	2.588	3.407	4.193	4.939	5.644	6.301	6.913
	15.750	11.464	8.326	7.028	6.208	5.523	4.247	1.478	-7.337
.7	H=-.9804	H=-.7895	H=-.5834	H= .0498	H= .3820	H= .6021	H= .7405	H= .8270	H= .8817
	***H	***H	***H	***H				**CL	CL.H
	.936	1.859	2.764	3.629	4.455	5.236	5.967	6.645	7.270
	17.196	11.140	8.783	8.026	7.739	7.442	6.800	5.203	-.149
.6	H=-.9875	H=-.8812	H=-.1769	H= .2673	H= .5568	H= .7314	H= .8317	H= .8910	H= .9270
	***H	***H	***H	***H	***H			**CL	CL.H
	1.010	2.006	2.972	3.893	4.774	5.594	6.353	7.052	7.690
	14.739	10.267	8.845	8.845	8.737	8.765	8.525	7.667	4.550
.5	H=-.9925	H=-.9161	H= .0712	H= .4835	H= .7128	H= .8343	H= .9004	H= .9368	H= .9584
	***H	***H	***H	***H	***H	***H	**CL	**CL	**CL
	1.106	2.193	3.242	4.231	5.173	6.036	6.827	7.544	8.191
	11.915	9.204	8.765	9.084	9.430	9.041	8.621	9.209	7.529
.4	H=-.9907	H=-.9463	H= .3504	H= .6918	H= .8366	H= .9104	H= .9476	H= .9676	H= .9790
	***H	***H	***H	***H	***H	**CL	**CL	**CL	**CL
	1.236	2.444	3.601	4.688	5.691	6.604	7.425	8.156	8.805
	9.328	8.152	8.633	9.259	9.703	10.013	10.071	9.904	9.120
.3	H=-.7710	H= .0934	H= .6304	H= .8416	H= .9247	H= .9605	H= .9776	H= .9864	H= .9913
	***H	***H	***H	***H	***H	**CL	**CL	**CL	**CL
	1.425	2.809	4.115	5.311	6.405	7.389	8.213	8.947	9.581
	6.297	7.161	8.276	9.010	9.421	9.619	9.699	9.684	9.447
.2	H=-.6596	H= .5185	H= .8571	H= .9463	H= .9761	H= .9870	H= .9933	H= .9960	H= .9975
	***H	***H	***H	***H	CL.H	CL.H	**CL	**CL	**CL
	1.741	3.407	4.987	6.301	7.480	8.481	9.322	10.024	10.608
	3.799	5.656	6.766	7.387	7.725	7.984	8.219	8.405	8.554
.1	H= .7337	H= .9066	H= .9781	H= .9925	H= .9969	H= .9985	H= .9992	H= .9995	H= .9997
	***H	***H	CL.H	CL.H	CL.H	CL.H	CL.H	**CL	**CL
	2.444	4.888	6.604	8.156	9.376	10.320	11.049	11.614	12.055
	.1	.2	.3	.4	.5	.6	.7	.8	.9

V RATIO

SI= 172.7060 AR=1.21 WT= .0333 HH= 3.00 HWS= .0400

TABLE 2 – SAMPLE ACCELERATION MAP

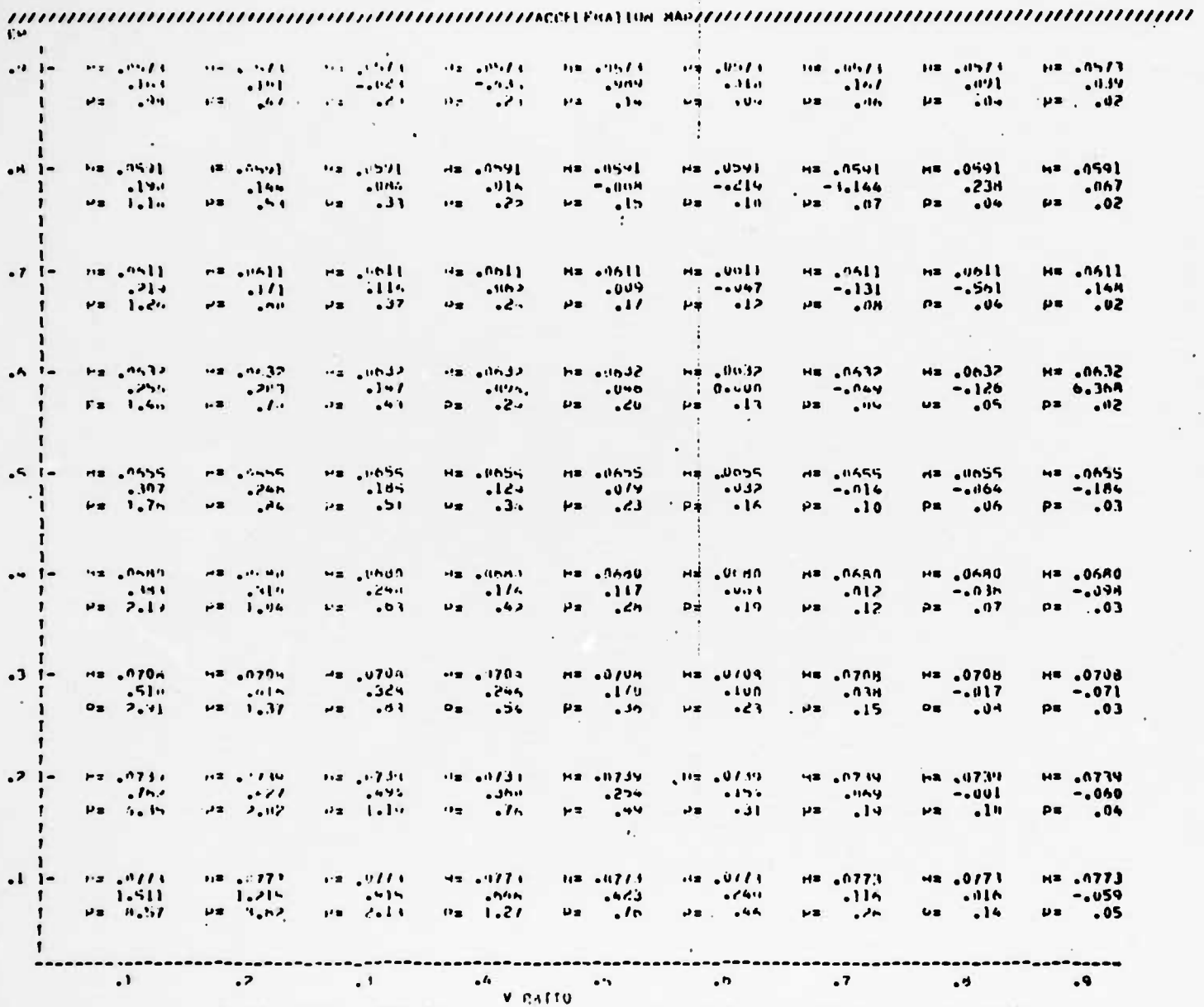

DTNSRDC ISSUES THREE TYPES OF REPORTS

(1) DTNSRDC REPORTS, A FORMAL SERIES PUBLISHING INFORMATION OF PERMANENT TECHNICAL VALUE, DESIGNATED BY A SERIAL REPORT NUMBER.

(2) DEPARTMENTAL REPORTS, A SEMIFORMAL SERIES, RECORDING INFORMATION OF A PRELIMINARY OR TEMPORARY NATURE, OR OF LIMITED INTEREST OR SIGNIFICANCE, CARRYING A DEPARTMENTAL ALPHANUMERIC IDENTIFICATION.

(3) TECHNICAL MEMORANDA, AN INFORMAL SERIES, USUALLY INTERNAL WORKING PAPERS OR DIRECT REPORTS TO SPONSORS, NUMBERED AS TM SERIES REPORTS; NOT FOR GENERAL DISTRIBUTION.


ATE
ME